Surface load induced electrical impedance shift in relaxor-PbTiO3 crystal piezoelectric resonators

Kyungrim Kim, Shujun Zhang, and Xiaoning Jiang

Related Articles

Additional information on Appl. Phys. Lett.

Surface load induced electrical impedance shift in relaxor-PbTiO₃ crystal piezoelectric resonators

Kyungrim Kim,[1] Shujun Zhang,[2] and Xiaoning Jiang[1,a)]

[1]Department of Mechanical and Aerospace Engineering, North Carolina State University, Raleigh, North Carolina 27695, USA
[2]Materials Research Institute, Pennsylvania State University, University Park, Pennsylvania 16802, USA

The effect of surface loads on Pb(Mg$_{1/3}$Nb$_{2/3}$)O$_3$-PbTiO$_3$ single crystal piezoelectric resonators was studied. Electrical impedance shifts at both resonance and anti-resonance frequencies due to surface loads were recorded for comparison among face-shear mode, thickness-shear mode, and thickness mode resonators. It was observed that electrical impedances of face shear mode resonators exhibited significantly higher sensitivity to surface load changes comparing with other resonators with similar dimensions, because of enhanced energy dissipation in face shear mode resonators, indicating a promising innovative face-shear mode single crystal piezoelectric sensing mechanism. © 2012 American Institute of Physics. [http://dx.doi.org/10.1063/1.4729766]

Relaxor-PbTiO$_3$ (PT) single crystals, including Pb(Mg$_{1/3}$Nb$_{2/3}$)O$_3$-PT (PMN-PT) and Pb(In$_{0.5}$Nb$_{0.5}$)O$_3$-Pb(Mg$_{1/3}$Nb$_{2/3}$)O$_3$-PT (PIN-PMN-PT), are known with advanced properties such as higher piezoelectric coefficients (e.g., $d_{33} > 1500$ pC/N), elastic constants (e.g., $s_{33}^E > 50$ pm^2/N), and electromechanical coupling factors (e.g., $k_{33} > 0.9$) when compared to Pb(Zr,Ti)O$_3$ (PZT) and other piezoelectric polycrystalline materials.[1–3] These crystals have been deployed successfully in piezoelectric sensors, actuators, and transducers for a broad range of applications.[4–6] More recently, the face-shear mode relaxor-PT crystals have drawn research attention due to their high piezoelectric coefficients (e.g., d_{36} of 1600-2800 pC/N) and ultrahigh elastic compliances ($s_{66}^E > 120$ pm^2/N). More importantly, unlike thickness shear mode crystals, the face shear mode crystals were found to possess much higher mechanical quality factor Q_m (>120, compared to ~30 for thickness shear mode crystals) and can be easily repolarized since the poling electrodes are the same as the active electrodes.[7] These unique properties suggest the need of further study on face shear mode single crystals for potential advanced applications. This letter investigates the effect of surface load on the face-shear mode PMN-PT single crystal resonators. The electrical impedance changes induced by the applied surface loads were measured and then the sensitivity or the ratio of electrical impedance change to the surface load variations was calculated and compared among thickness mode, thickness-shear mode, and face-shear mode single crystal piezoelectric resonators. Finally, the experimental results were verified by an analytical model, followed by discussions.

For face shear resonators, [011] poled rhombohedral PMN-PT single crystals were used, which possess the macroscopic symmetry mm2. Face-shear mode plates (10 mm × 10 mm × 1 mm) were prepared by rotating a 45° angle about the Z-axis [011] direction. Cr/Au electrodes were deposited on (011) surface of each resonator plate. The 10 cm co-ax wires (AWG 25) were bonded to electrode surfaces using silver epoxy for electrical connection. For the

prepared crystal samples, the capacitance, resonant frequency, and anti-resonant frequency were measured using an impedance analyzer (HP4294A, Agilent). According to the IRE standards,[8,9] properties of the face-shear PMN-PT single crystals can be calculated. Similarly, thickness-shear (10 mm × 10 mm × 1 mm) and thickness (10 mm × 10 mm × 0.5 mm) mode PMN-PT crystals were prepared and characterized for the following surface load experiments. The poling direction, electrodes, and vibration mode for prepared single crystal resonators in three different modes were shown in Fig. 1. Both acoustic surface load and surface force load experiments were performed using the prepared resonators. In order to apply different surface acoustic loads, alumina (Al$_2$O$_3$) powders in different percentages by weight were mixed with the liquid silicone rubber (Sylgard 170, Dow Corning Corp.). The liquid silicone rubber (about 2 mm thick) with and without Al$_2$O$_3$ powders (10%, 20%, 30%, and 40% of the silicone rubber by weight) was applied to one large surface (10 mm × 10 mm) of each crystal resonator plate and cured for 24 h in a vacuum desiccator. Acoustic impedances of rubber mixtures were characterized by measuring sound velocity and density of rubber mixtures. The longitudinal sound speed of rubber mixtures was measured using the ultrasonic pulse-echo method. The time of flight of echo waves received by a 30 MHz transducer from the top and bottom surfaces of rubber samples (2 mm thick) was recorded and the longitudinal sound velocity was then calculated.[10] The shear velocity (v_s) of rubber mixtures was
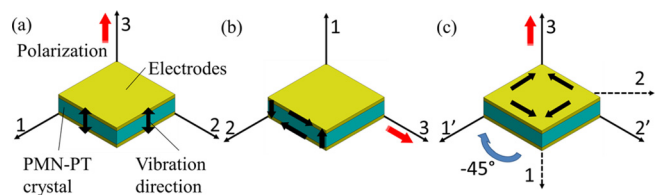

FIG. 1. The poling direction, electrodes, and vibration mode for (a) thickness mode, (b) thickness-shear mode, and (c) face-shear mode PMN-PT crystals.

a)Electronic mail: xjiang5@ncsu.edu.

calculated from the longitudinal velocity using the Poisson's ratio of rubbers ($v = 0.5$). The density of the rubber mixtures (ρ) was calculated using measured volume and weight. Finally, the shear acoustic impedance (Z_s) of rubber mixtures, or surface loads, was calculated ($Z_s = \rho v_s$), which was found to increase with weight percentages of Al_2O_3 powders in rubber mixtures.

The electrical impedance spectra for face-shear, thickness-shear, and thickness mode resonators under different surface loads were measured using an impedance analyzer. In order to verify the measured electrical impedance results, electrical impedances (Z_{AB}) for loaded and unloaded piezoelectric crystal resonators were also estimated using the transmission line Krimholtz, Leedom, and Matthaei model (KLM model) as follows:[11,12]

$$Z_{AB} = \frac{1}{j\omega C_0}\left[1 - \frac{k^2}{\alpha}\frac{2\tan\frac{\alpha}{2} - j\frac{Z_L}{Z_c}}{1 - j\frac{Z_L}{Z_c}\cot\alpha}\right], \quad (1)$$

where ω, C_0, k, α, and Z_c represent the angular frequency, clamped capacitance of the crystal plate, electromechanical coupling factor, the complex acoustic wave phase shift ($= \pi\omega/\omega_0$, ω_0 is anti-resonant frequency), and the acoustic impedance of the piezoelectric crystal ($= A\rho v$, A is the aperture area, ρ is the density, and v is the sound speed of the crystal), respectively. The ratio (S_z) of electrical impedance shift (ΔZ_{AB}) of crystal resonators to the applied surface load change or acoustic impedance change (ΔZ_L) can be considered as the electrical impedance sensitivity to surface acoustic load for the studied crystal resonators.

For resonator tests under various applied forces, a layer of pure silicone rubber was applied to both large surfaces of crystal resonator plates. Weight forces were then applied to the rubber layer through a steel cylinder. Similarly, the ratio (S_F) of electrical impedance shift (ΔZ_{AB}) to applied force change (ΔF_S) can be considered as the electrical impedance sensitivity to surface force loads for the studied crystal resonators.

Figures 2(a) and 2(b) present the results of measured and calculated electrical impedance changing with acoustic load impedance for PMN-PT resonators in three different modes at resonant frequency and anti-resonant frequency, respectively. One can observe that for the face-shear mode resonator, the electrical impedance increases and decreases rapidly with the increasing acoustic impedances of surface loads at the resonant frequency and anti-resonant frequency, respectively. This is in stark contrast to the findings from

TABLE I. Properties of relaxor-PT single crystals for the calculation.

PMN-PT	Dim. (mm^3)	f_a	k_{ij}	C_0 (nF)	Z_C (Mrayl)
Thickness mode (d_{33})	$10 \times 10 \times 0.5$	5.0 MHz	0.58 (k_t)	1.6	40.5
Thickness-shear mode (d_{15})	$10 \times 10 \times 1$	1.2 MHz	0.90	1.1	19.4
Face-shear mode (d_{36})	$10 \times 10 \times 1$	93.5 kHz	0.76	1.1	15.2

thickness and thickness-shear mode resonators with similar sizes. In specific, the ratio of electrical impedance shift to the applied acoustic impedance of the face-shear mode resonator was found to be at least 20 times and 90 times higher than those of thickness-shear mode and thickness mode resonators, respectively. Table I indicates the properties of three different PMN-PT crystals used for the calculation. The slight difference between the measured and calculated results is likely due to the fact that the effect of additional surface loads from the wires and silver epoxy used for the wire bonding was not considered in the simulation. Figures 3(a) and 3(b) show measured electrical impedances under different surface forces for resonators in three modes, at the resonant frequency and anti-resonant frequency, respectively. Again, significantly higher electrical impedance shift sensitivity (S_F) under applied surface forces was observed from the face-shear mode resonator at both resonance and anti-resonance frequencies, comparing with S_F observed from thickness mode and thickness shear mode resonators. These findings (Figs. 2 and 3) can be supported by the nature of advanced properties of face-shear mode crystals. The crucial factors which determine the electrical impedance characteristic of piezoelectric resonators are the frequency (ω), clamped capacitance C_0, acoustic load (Z_L), and acoustic impedance of resonators (Z_C) as shown in Eq. (1). The anti-resonant frequency ($\omega_0 = \pi v/t$ or $\pi v/l$) and the static capacitance ($C_0 = \varepsilon A/t$) are related with the resonator dimension (t and l), and the product of them ($= \omega_0 C_0$) affects resultant electrical impedance at resonance and anti-resonance. As the magnitude of $\omega_0 C_0$ decreases, the slope ($|\Delta Z_{AB}/\Delta Z_L|$) of electrical impedance shift over acoustic load increases as shown in Figs. 4(a) and 4(b), indicating that electrical impedance shift of face shear mode resonators is significantly more sensitive to surface load changes comparing with resonators in other two modes. The small inset in Fig. 4(b) indicates the relationship between $\omega_0 C_0$ and the crystal aspect ratio for three different modes. In square plate (dimensions: $l \times l \times t$) resonators, the frequency
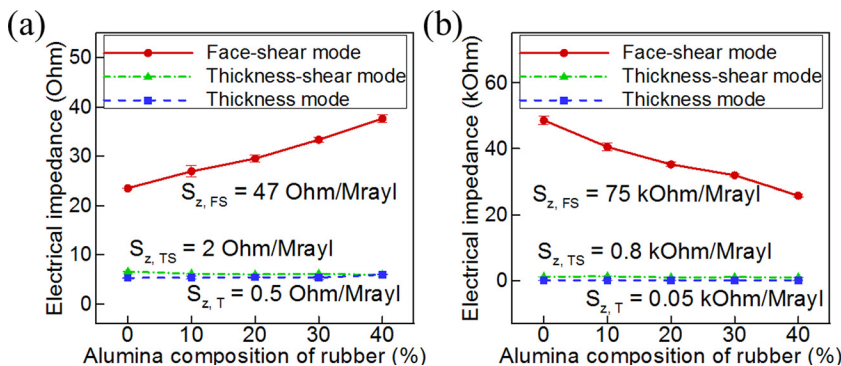

FIG. 2. Comparison of measured electrical impedance (Z_{AB}) and sensitivity (S_z) under different surface loads for face-shear mode (FS), thickness-shear mode (TS), and thickness mode (T) resonators. (a) Measured electrical impedance at the resonant frequency. (b) Measured electrical impedance at the anti-resonant frequency. (Calculated sensitivities at the resonant frequency for three different mode resonators: $S_{z,FS} = 88\ \Omega/\text{Mrayl}$, $S_{z,TS} = 2.1\ \Omega/\text{Mrayl}$, and $S_{z,T} = 0.7\ \Omega/\text{Mrayl}$. Calculated sensitivities at the anti-resonant frequency: $S_{z,FS} = 46\ \text{k}\Omega/\text{Mrayl}$, $S_{z,TS} = 0.8\ \text{k}\Omega/\text{Mrayl}$, and $S_{z,T} = 0.3\ \text{k}\Omega/\text{Mrayl}$).
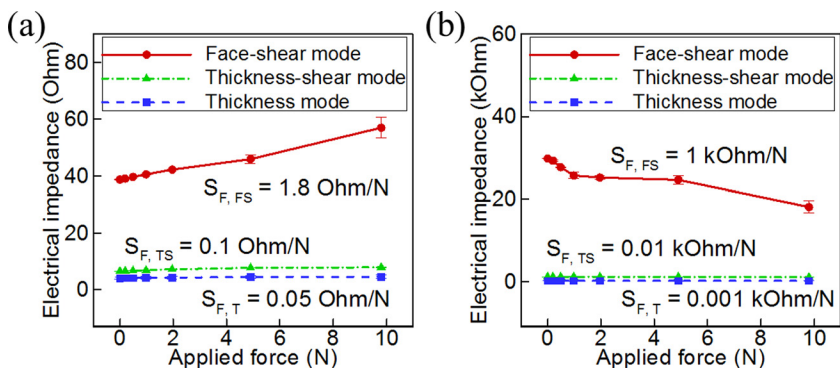
FIG. 3. Comparison of measured electrical impedance (Z_{AB}) and sensitivity (S_F) under different surface forces (0.2 N–10 N) for FS mode, TS mode, and thickness mode (T) resonators. (a) Measured electrical impedance at the resonant frequency. (b) Measured electrical impedance at the anti-resonant frequency.
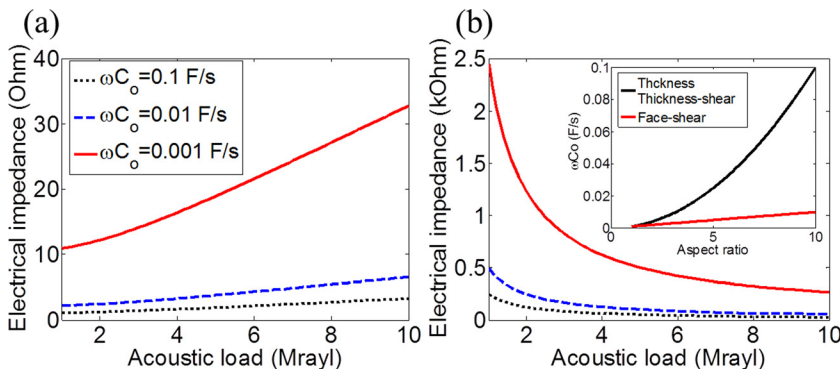

FIG. 4. (a) Calculated electrical impedance (Z_{AB}) as a function of acoustic load (Z_L) at the resonant frequency and (b) calculated electrical impedance at the anti-resonant frequency. The small inset in (b) indicates the relationship between ωC_0 and the aspect ratio (l/t) of crystal dimensions. For the calculation, electromechanical coupling factor (k) and characteristic impedance (Z_C) are 0.8 and 30 Mrayl, respectively.

determining factor of thickness and thickness-shear mode is the crystal thickness (t), while that of face-shear-mode is the lateral length (l). $\omega_0 C_0$ can be expressed by $\pi \varepsilon v (l/t)^2$ for thickness and thickness-shear mode, and $\pi \varepsilon v (l/t)$ for face-shear mode. As a result, face-shear mode resonator is featured with lower $\omega_0 C_0$ than other modes with the same aspect ratio ($l:t$) and thus its electrical impedances at both resonance and anti-resonance frequencies shift more rapidly under surface loads. On the other hand, the low acoustic impedance of the loaded crystal (Z_C) can lead to a significant change in electrical impedance at the resonant frequency, while no significant change was found at the anti-resonant frequency, as can be seen in Figs. 5(a) and 5(b). This also can affects the load sensitivity of resonators at the resonant frequency since Z_C of each resonator is different (Table I). Nevertheless, the load sensitivity of face-shear mode resonator is affected dominantly by the product of the angular frequency and the static capacitance at both resonance and anti-resonance, due to more than two orders of magnitude difference in $\omega_0 C_0$ between face-shear mode and other modes. The electromechanical coupling factor (k) affects

the resonant frequency shift but not the magnitude of electrical impedance change. Besides, α in Eq. (1) does not play a significant role in determining the electrical impedance change since α is constant near the resonant frequency ($\alpha = \pi \omega_r / \omega_0$) and the anti-resonance frequency ($\alpha = \pi \omega_0 / \omega_0$). For surface force tests, the applied force (F_S) through the rubber layer on top of the resonator surface can be considered as a clamping force leading to vibration energy losses. As high clamping force is applied, more energy is dissipated, resulting in decreased Q_m and electrical impedance changes in crystal resonators. Unlike thickness and thickness-shear mode, the particle vibration of the face-shear mode resonator occurs along the diagonal axis on the large surfaces (or loaded surfaces). Therefore, when the face-shear resonator is clamped by applied surface force (F_S), relatively high energy dissipation occurs on its surface which can result in the large reduction of mechanical quality factor (Q_m) of the resonator. Consequently, the electrical impedance (Z_{AB}) increases at the resonance and decreases at the anti-resonance, with weak resonance peaks corresponding to the reduced Q_m.
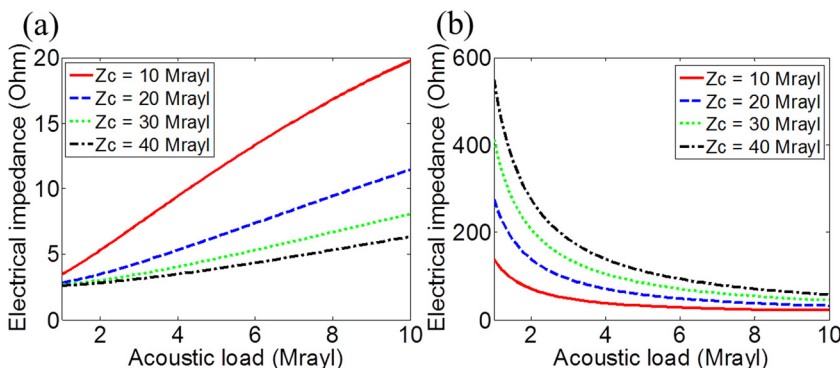

FIG. 5. (a) Calculated electrical impedance (Z_{AB}) with different characteristic impedance of the resonator at the resonant frequency and (b) calculated electrical impedance with different characteristic impedance at the anti-resonant frequency. For the calculation, electromechanical coupling factor (k) and the value of ωC_0 are 0.8 and 0.01 F/s, respectively.

In summary, the effect of surface loads on PMN-PT single crystal piezoelectric resonators was investigated. Different acoustic surface loads were applied to the thickness mode, thickness-shear mode, and face-shear mode resonators with similar dimensions. The highest sensitivity of electrical impedance to the surface loads, including rubber mixtures with different acoustic impedances and applied forces, was obtained from the face-shear resonator. The experimental results were in general agreement with the analytical estimations. These findings suggest that more energy dissipation occurs in face shear resonators under surface loads. The newly revealed characteristic of high sensitivity of electrical impedance to surface loads for face shear mode resonators can be favorable for a number of applications, including smart artificial skins, biological sensors, chemical sensors, touch screen, and other tactile based sensors.

[1] S. Zhang and F. Li, J. Appl. Phys. **111**, 031301 (2012).
[2] D. Zhou, J. Chen, L. Luo, X. Zhao, and H. Luo, Appl. Phys. Lett. **93**, 073502 (2008).
[3] S. Zhang, F. Li, N. P. Sherlock, J. Luo, H. J. Lee, R. Xia, R. J. Meyer, Jr., W. Hackenberger, and T. R. Shrout, J. Cryst. Growth **318**, 846 (2010).
[4] K. C. Cheng, H. L. W. Chan, C. L. Choy, Q. Yin, H. Luo, and Z. Yin, IEEE Trans. Ultrason. Ferroelectr. Freq. Control **50**, 1177 (2003).
[5] P. A. Wlodkowski, K. Deng, and M. Kahn, Sens. Actuators, A **90**, 125 (2001).
[6] S. Dong, L. Yan, N. Wang, D. Viehland, X. Jiang, P. Rehrig, and W. Hackenberger, Appl. Phys. Lett. **86**, 053501 (2005).
[7] S. Zhang, F. Li, W. Jiang, J. Luo, R. J. Meyer, W. Cao, and T. R. Shrout, Appl. Phys. Lett. **98**, 182903 (2011).
[8] IRE Standards on Piezoelectric Crystals, Proc. IRE **46**, 764 (1958).
[9] S. Zhang, W. Jiang, R. J. Meyer, F. Li, J. Luo, and W. Cao, J. Appl. Phys. **110**, 064106 (2011).
[10] I. Y. Kuo, B. Hete, and K. K. Shung, J. Acoust. Soc. Am. **88**, 1679 (1990).
[11] R. Krimholtz, D. A. Leedom, and G. L. Matthaei, Electron. Lett. **6**, 398 (1970).
[12] R. W. Cernosek, S. J. Martin, A. R. Hillman, and H. L. Bandey, IEEE Trans. Ultrason. Ferroelectr. Freq. Control **45**, 1399 (1998).